Valence change detection in memristive oxide based heterostructure cells by hard X-ray photoelectron emission spectroscopy

A. Kindsmüller, C. Schmitz, C. Wiemann, K. Skaja, D. J. Wouters, R. Waser, C. M. Schneider, and R. Dittmann

Citation: APL Materials **6**, 046106 (2018); doi: 10.1063/1.5026063
View online: https://doi.org/10.1063/1.5026063
View Table of Contents: http://aip.scitation.org/toc/apm/6/4
Published by the American Institute of Physics

Valence change detection in memristive oxide based heterostructure cells by hard X-ray photoelectron emission spectroscopy

A. Kindsmüller,[1,a] C. Schmitz,[2] C. Wiemann,[2] K. Skaja,[2] D. J. Wouters,[1] R. Waser,[1,2] C. M. Schneider,[2] and R. Dittmann[2,b]
[1]*Institute of Materials in Electrical Engineering and Information Technology II (IWE2), RWTH Aachen, 52056 Aachen, Germany*
[2]*Peter Gruenberg Institute, Forschungszentrum Juelich GmbH, 52425 Juelich, Germany*

(Received 15 February 2018; accepted 7 April 2018; published online 20 April 2018)

The switching mechanism of valence change resistive memory devices is widely accepted to be an ionic movement of oxygen vacancies resulting in a valence change of the metal cations. However, direct experimental proofs of valence changes in memristive devices are scarce. In this work, we have employed hard X-ray photoelectron emission microscopy (PEEM) to probe local valence changes in Pt/ZrO_x/Ta memristive devices. The use of hard X-ray radiation increases the information depth, thus providing chemical information from buried layers. By extracting X-ray photoelectron spectra from different locations in the PEEM images, we show that zirconia in the active device area is reduced compared to a neighbouring region, confirming the valence change in the ZrO_x film during electroforming. Furthermore, we succeeded in measuring the Ta 4f spectrum for two different resistance states on the same device. In both states, as well as outside the device region, the Ta electrode is composed of different suboxides without any metallic contribution, hinting to the formation of TaO_x during the deposition of the Ta thin film. We observed a reduction of the Ta oxidation state in the low resistance state with respect to the high resistive state. This observation is contradictory to the established model, as the internal redistribution of oxygen between ZrO_x and the Ta electrode during switching would lead to an oxidation of the Ta layer in the low resistance state. Instead, we have to conclude that the Ta electrode takes an active part in the switching process in our devices and that oxygen is released and reincorporated in the ZrO_x/TaO_x bilayer during switching. This is confirmed by the degradation of the high resistance state during endurance measurements under vacuum. https://doi.org/10.1063/1.5026063

Redox-based memristive devices (ReRAM) are considered as one of the most promising emerging memory technologies, even allowing multibit operation, logic-in-memory, and neuromorphic computing applications.[1–3] In these devices, the resistance of an oxide layer sandwiched between two metal electrodes can be modified by an external electrical stimulus between two or more resistance states. The underlying mechanism, which is called the valence change mechanism, is widely accepted to be a nanoscale redox reaction, induced by the movement of mobile donor-type defects such as oxygen vacancies.[1,2] Despite the increasing knowledge about the microscopic mechanisms over the past years, many open questions remain due to the fact that the relevant chemical changes are confined to nanoscale filaments and/or to the electrode-oxide interface. A variety of spatially resolved, spectroscopic techniques such as photoelectron emission microscopy (PEEM),[4–6] transmission X-ray spectroscopy,[7–9] and electron energy loss spectroscopy[10,11] have been employed to study the electronic structure of active filaments in ReRAM devices.[12] By employing soft X-ray PEEM,

[a]E-mail: kindsmueller@iwe.rwth-aachen.de
[b]E-mail: r.dittmann@fz-juelich.de

a change of the metal valence state during resistive switching has been proven for $SrTiO_3$[5,6,13] and Ta_2O_5.[14] The drawback of this technique is that the mean-free path of photoelectrons excited in the soft X-ray regime is on the order of a few nanometers. This problem has been tackled by peeling-off of the top electrode prior to the spectroscopic measurement[15] or by the use of electron-transparent graphene electrodes.[5] Thanks to its larger probing depth (>10 nm), hard X-ray photoemission spectroscopy (HAXPES) provides an excellent, nondestructive approach to probe chemical changes of interfaces buried inside layered heterostructures and thereby allows the investigation of ReRAM cells with conventional metallic electrodes.[16–19] Whereas HAXPES analysis on large area cells has been successful in detecting valence changes in non-filamentary switching systems,[20] it failed to detect valence changes in filamentary systems such as HfO_2[21] and TiO_2[22] as a result of the insufficient amount of modified material in the cell.

In this work, we employed hard X-ray PEEM (HAXPEEM) to detect chemical changes in ZrO_x ReRAM cells with improved spatial resolution as compared to HAXPES. Our ZrO_x ReRAM cells contain one noble metal electrode such as Pt or Rh, which is expected to provide the active Schottky interface[23] and one oxidizable electrode, namely Ta, which is expected to form an interfacial oxide layer by extracting oxygen from the ZrO_x film.[24] In the simplest case, the resulting interface oxide layer acts as an oxygen reservoir but is not actively involved in the switching process. However, recent investigations have pointed out a strong involvement of the reactive electrode in the switching process[25,26] and the switching kinetics.[27] Indications for this involvement have also been found by scalpel scanning probe microscopy[28,29] and TEM.[9] In order to assign redox processes within both the ZrO_x and Ta layers to the observed resistance change, we performed HAXPEEM investigations of noble metal/ZrO_x/Ta ReRAM devices with different layer sequences. This enabled us to prove the involvement of the TaO_x interface layer in the switching process, suggesting an oxygen exchange reaction of the TaO_x layer with the surrounding atmosphere[10] as the switching mechanism rather than an internal redistribution of oxygen.

The instrument used in this study is an energy-filtering photoemission microscope based on a Focus NanoEsca,[30] which was customized for the use with hard X-ray excitation.[31,32] In short, the photoemission microscope is used as magnifying entrance optics for a double hemispherical analyser. It provides a bandpass filter for the kinetic energy of the electrons used to image the sample in real space. Photoelectron spectroscopy at a spatial resolution of ~400 nm has been demonstrated. The use of hard x-rays results in electron kinetic energies of several keV, which increases the electron attenuation length and hence the probing depth to 10-15 nm. Measurements were carried out at beamline P09 at synchrotron PETRAIII, DESY, Hamburg, Germany.[33]

The use of HAXPEEM imposes several special requirements to the sample design of a ReRAM cell. In order to retrieve chemical information from the full device, the total thickness of the active stack (top electrode plus oxide thickness) should be less than the probing depth, which is in the range of 10–15 nm. As the switching usually happens at the interface of the noble metal electrode to the oxide, it would be best to get the strongest PEEM signal from this interface. Hence, this interface should be as close to the surface as possible.

For the experiments, two different sample stacks were fabricated and tested: a Pt (bottom)/ZrO_x/Ta/Pt (top) stack ("Ta-top-stack") and a Pt (bottom)/Ta/ZrO_x/Rh (top) stack ("Ta-bottom-stack"). The device geometry used for both the stacks is depicted in Fig. 1(a) on the example of a "Ta-bottom-stack." We used a 2 nm thin noble top electrode topped with a 30 nm Pt finger with only 2 μm overlap to guarantee good electrical contact to the device but still maintain a large observable area with PEEM. Details of the sample preparation can be found in the supplementary material. The overall cross section of the "Ta-bottom" and "Ta-top" stacks is shown in Figs. 1(b) and 1(c), respectively.

Prior to the HAXPEEM analysis, the samples were characterized electrically in detail. Figure 2 shows *I*-*V*-sweeps of the two different devices. The switching direction changes when the order of the layers is reversed since the position of the active interface (noble electrode-ZrO_x) is changed between the top and the bottom interface. The SET process [switching from high resistance state (HRS) to the low resistance state (LRS)] always happens at a negative bias to the noble electrode-ZrO_x interface. For both types of stacks, the devices show stable, reproducible switching (up to 100 cycles per cell) and no effect of the cycling on the switching characteristics was observed. It is important

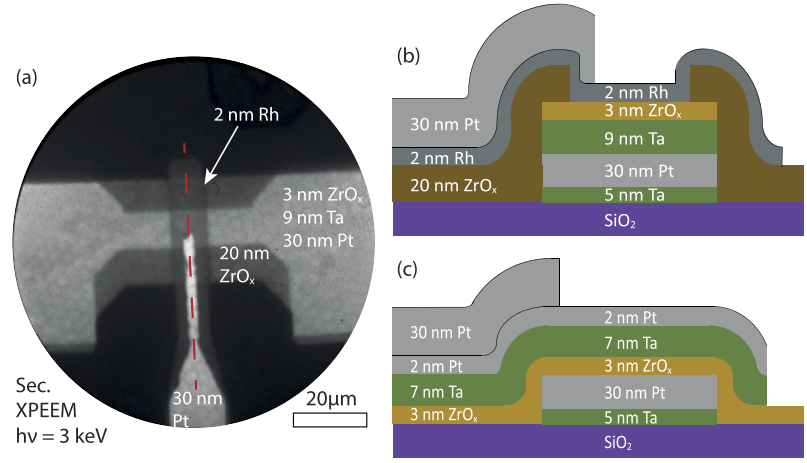

FIG. 1. (a) Secondary electron XPEEM image showing the structure of a "Ta-bottom"-device. The different materials present at each feature are indicated. (b) Cross section along the red line in (a) of a "Ta-bottom"-device. (c) Cross section along the red line in (a) of a "Ta-top"-device.

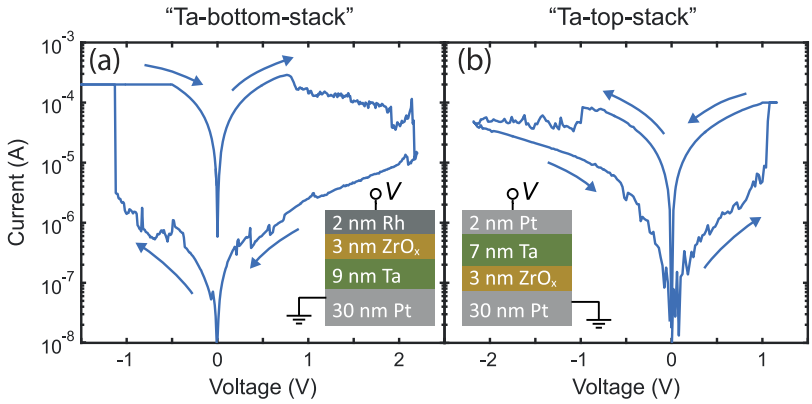

FIG. 2. An example of an *I*-*V*-sweep of (a) a "Ta-bottom" device and (b) a "Ta-top" device. Both devices show well pronounced bipolar switching behavior. The corresponding stacks are depicted in the insets.

to note that the retention of the "Ta bottom" devices in air is relatively short, the LRS state usually approaches the HRS within an hour. This is likely caused by the fact that the 2 nm top electrode is too thin to prevent the reoxidation of the oxygen deficient filament within the ZrO_x layer formed during the SET process.[13] In vacuum, both states are stable over 2 days, which is absolutely sufficient for the HAXPEEM measurements (cf. Fig. S1 of the supplementary material). The endurance is higher than 10^3 cycles in air and vacuum.

In a first approach, the samples were switched *ex situ*, meaning that the different resistance states were achieved in air using a needle contact outside the PEEM analysis chamber. These predefined resistance states were subsequently transferred into the HAXPEEM UHV chamber and characterized. Figure 3(a) shows the lateral distribution of the Zr 3d XPS core level intensity [X-ray PEEM (XPEEM) image] after a principle component analysis[34] of a "Ta bottom" device in the LRS. The structure of the device is clearly recognizable. Even after 3 h of integration, the signal acquired from a field of view (FoV) of about 40 μm remains noisy, and thus only large areas can be evaluated, which leads to an effective reduction in the lateral resolution. The evaluation of the spectra in single pixels is impossible due to the low signal intensity. Nonetheless, a comparison of the active junction area—where the actual switching takes place—and a neighbouring reference area provides interesting results. Figure 3(b) shows the reference XPS spectra extracted from the green marked region in Fig. 3(a). It can be fitted

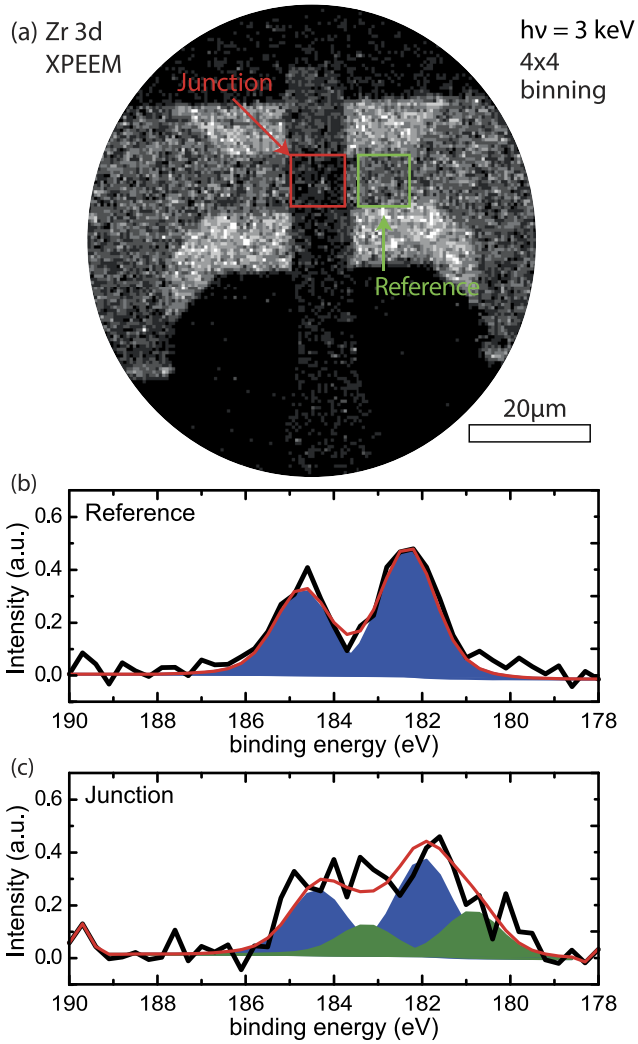

FIG. 3. (a) XPEEM image visualizing the intensity of the Zr3d spectrum of a "Ta-bottom"-device. The image is the result of a principle component analysis and binned 4×4 pixels to increase statistics. The signal at the junction area (red) is compared with a reference signal (green area). (b) In the reference area, the XPS signal can be fitted well with a simple doublet corresponding to Zr^{4+} as in ZrO_2. (c) In the junction area, the signal has a shoulder to lower binding energies. This corresponds to a reduced component, likely Zr^{3+}.

with a simple doublet corresponding to the spin-orbit splitted Zr 3d main line as expected for ZrO_2. The spectrum of the junction region [cf. Fig. 3(c), extracted from the red square in Fig. 3(a)] has a lower intensity as it is buried underneath 2 nm Rh. The initial oxidation state in the two regions should be the same, as both areas have the same bottom interface (Ta—ZrO_x), and the evaporation of the Rh top electrode at the junction should not change the stoichiometry of the underlying ZrO_x layer. The whole ZrO_x layer was exposed to air before the Rh deposition so that an influence of reoxidation on the change of the oxidation state in the junction can also be excluded. The Zr 3d spectrum in the junction clearly shows a wider energy distribution and a shoulder toward lower binding energies. This effect is not due to electrostatic charging, as the Pt core level spectra of the top and bottom electrodes are not shifted with respect to each other. It can be fitted with an additional doublet, which is at a binding energy 1.1 eV lower than the binding energy of the Zr 3d spectrum of the fully oxidized ZrO_2. A shift by this energy has been reported in the literature[35] and was attributed to the Zr^{3+} component. This is in good agreement with the common explanation that the switching in transition metal oxide based ReRAM cells is due to a local reduction of the oxide layer (oxygen vacancy filament).[23] According to an expected size of the filament of less than 100 nm, the spatial resolution at the given experimental

conditions is insufficient to resolve the filament, but the net oxygen vacancy concentration in the cell area is sufficiently high to be detected.

The evaluation of the *in situ* measurement of the "Ta-bottom" cells was impossible, as most of the devices were shorted after the beam irradiation. The few devices which did not change their resistance state during the irradiation could not be switched afterwards, and a characterization of the different states was hence impossible. In contrast, the "Ta-top-devices" were less susceptible to beam damage and retained their resistance state after beam irradiation, but spectroscopic data could only be acquired for the Pt (top and bottom) and Ta layers. No signal could be retrieved from the ZrO_x-layer as it was buried under a 9 nm thick Ta/Pt stack, only 3 nm thin, and the photoionization cross section of Zr 3d is lower than the one of Pt 4f at this photon energy.[36]

For one of the "Ta-top-devices," the Ta 4f spectrum of a high resistance state and a low resistance state could be acquired after *in situ* switching in between the two measurements. The comparison of the Ta 4f spectra of the active junction area in the two different resistance states is shown in Fig. 4(a). The major peak is at a binding energy of 26.7 eV, which corresponds to the Ta 4f peak of Ta_2O_5. Furthermore, the spectrum has a broad shoulder toward lower binding energy but apparently no metallic component which should be located at 21.9 eV. The direct comparison of the two spectra

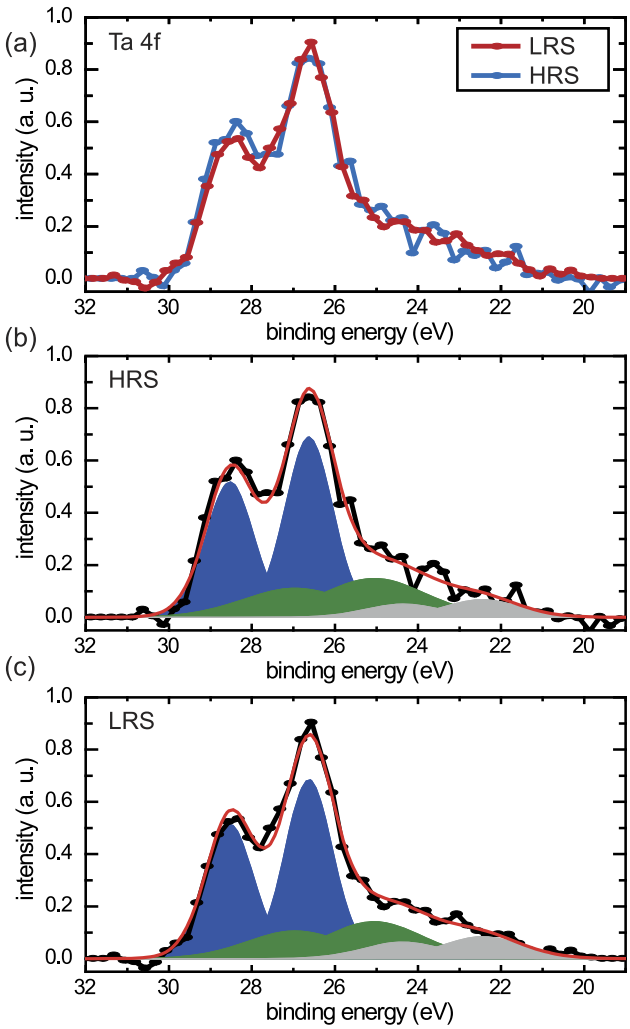

FIG. 4. (a) Comparison between the HRS (blue) and the LRS (red) of the Ta 4f spectra of the same device. The peak with the highest binding energy is enhanced in the HRS. (b) Fitting of the HRS spectrum with a TaO_{1-x}, TaO_{2-x}, and Ta_2O_5 component. Black represents the measured data, and red is the envelope of the fitted data. (c) Equivalent fitting of the LRS state.

TABLE I. Contributions of the different Ta 4f-peaks in the LRS and HRS.

Component	Corrected Ta 4f 7/2 energy (eV)	Contribution LRS (%)	Contribution HRS (%)
TaO_{1-x}	22.5	12.7	9.6
TaO_{2-x}	25.1	25.9	28.9
Ta_2O_5	26.7	61.4	61.5

shows a difference between the two states. To characterize this further, we fitted the peak shapes with the following Ta 4f components: Ta_2O_5, TaO_{2-x}, and TaO_{1-x} [cf. Figs. 4(b) and 4(c)]. The peak positions fit reasonably well with literature values.[37,38] The contribution of the different peaks and their energies can be found in Table I. Clearly, there is a shift from the TaO_{2-x} component to the TaO_{1-x} component, when the device is switched to the LRS. This means that there is more TaO_{2-x} in the HRS and hence more oxygen in the TaO_x layer than in the LRS.

It is important to note that even though the Ta-layer was sputtered from a metal target in pure Ar atmosphere, it is strongly oxidized. This is also the case for the as-deposited Ta-layer on SiO_2—see Fig. S2 of the supplementary material. The reasons for the observed oxidation can be various: (i) The residual oxygen gas in the chamber at the base pressure of 10^{-6} mbar probably results in the oxidation of the Ta layer during deposition. (ii) The target could be poisoned with oxygen as other processes in the same chamber are using oxygen atmospheres and can lead to an oxidation of the target and hence of the thin film deposited in a consecutive process. (iii) Additionally, the oxygen exchange at the interface with the ZrO_x layer leads to further oxidation in this stack.[39] This is also supported by measurements with different photon energies and hence probing depth. The Ta layer is oxidized most strongly at the interface with the ZrO_x layer—see Fig. S3 of the supplementary material. (iv) Furthermore, the 2 nm Pt top electrode is probably not a perfect diffusion barrier for oxygen in the atmosphere, resulting in an oxidation from the top interface.[13]

In the established switching model for valence change memory-type ReRAM devices, it is assumed that during the SET (negative voltage at the Pt-bottom-electrode) positively charged oxygen vacancies are pushed into the ZrO_x layer and form a filament resulting in a higher conductance of the layer stack. According to the large amount of suboxides in the TaO_x layer in both resistive states, one can assume that the top interface has an ohmic character and that the ZrO_x—Pt interface forms a Schottky-barrier. The ZrO_x—Pt interface can therefore be regarded as the active interface where the largest field drop takes place and the strongest change of the conductance during ionic motion is expected due to a change in tunnel barrier height and width. This is also consistent with the observed switching direction. In the LRS, one would expect that oxygen is incorporated into the Ta layer to compensate for the additional vacancies in ZrO_x. However, this is in conflict with our measurement since we observe a further reduction of the TaO_x in the LRS. The high oxygen content of the TaO_x layer could result in a high resistivity, causing a significant field drop over the layer. This means, in particular, that the oxygen vacancies start to move and the conducting filament is formed in both the TaO_x and ZrO_x layers, as depicted in Figs. 5(a) and 5(b). During the SET, there would be an increase in oxygen vacancies in both the ZrO_x and TaO_x layers, which goes along with a release of oxygen from the two layers. The released oxygen could be either stored as interstitials in the platinum or be released into the surrounding. This scenario is also supported by endurance measurements in vacuum [cf. Fig. 5(c)]. The HRS slowly degrades to lower resistance values, as there is less and less oxygen left for the reoxidation of the filament. A similar mechanism of oxygen release and reincorporation has already been suggested for other valence change memristive systems, such as WO_{3-x},[40] TiO_2,[41] Si-rich SiO_x[42,43] $SrTiO_3$,[10,13] CeO_2,[44] $SrRuO_3$,[45] $La_{0.8}Sr_{0.2}MnO_3$,[46] $Pr_{0.67}Ca_{0.33}MnO_3$[47] as well as for HfO_x[48,49] and TaO_x.[45]

We employed HAXPEEM analysis to detect chemical changes in two different memristive heterostructure stacks, namely, a Pt (bottom)/ZrO_x/Ta/Pt (top) stack ("Ta-top-stack") and a Pt (bottom)/Ta/ZrO_x/Rh (top) stack ("Ta-bottom-stack"). A spatially resolved Zr3d XPEEM image of the "Ta-bottom-device" shows that ZrO_x is reduced in the active device area compared to a neighbouring area. This confirms that oxygen is removed from the ZrO_x layer during the forming procedure. Furthermore, Ta 4f core-level spectra could be taken from the "Ta-top-stack" in the HRS and LRS.

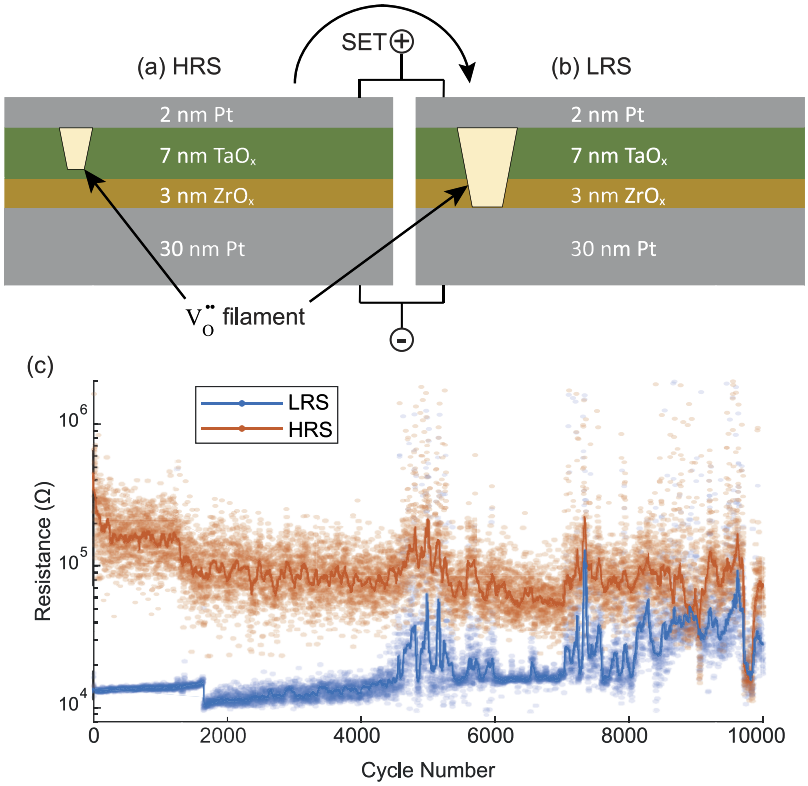

FIG. 5. Possible explanation of the measured effect. The Ta layer is strongly oxidized; hence, it acts as an insulator and the filament is formed through the whole film. (a) In the HRS, there are only a few oxygen vacancies left in the TaO_x layer. (b) During SET, new oxygen vacancies are introduced into both layers and lead to a reduction of both layers. (c) Resistance during an endurance measurement in vacuum, with the median over 50 measurements as solid line. The HRS resistance shows a strong degradation.

These measurements reveal that the Ta layer changes its oxidation state during switching. In particular, the comparison of the spectra in the two resistive states shows that the Ta layer in the LRS exhibits a shift to lower oxidation states of the Ta and hence contains less oxygen than in the HRS. As the layer is strongly oxidized in both states, it has to be assumed that the Ta layer is oxidized already during the deposition process. This results in a high resistivity, implying that the oxygen vacancy filament has to proceed into this layer in the LRS. Therefore additional oxygen vacancies are formed in the TaO_x layer during the SET process. As there is no other oxidizable material in the remaining stack, we have to conclude that oxygen is released and reincorporated during the switching process. The released oxygen might be partially stored in the Pt electrode and partially released to the environment. This switching process is consistent with a degradation of the HRS during endurance measurements in vacuum. Our experimental findings indicate that both the active oxide layers and the metal electrodes might undertake valence changes during device operation which have to be considered to explain the microscopic switching processes.

See supplementary material for the detailed description of the sample preparation, a retention measurement of a "Ta-bottom" device in vacuum, and an XPS spectrum of the as-deposited Ta layer. Furthermore, an analysis of the Ta layer oxidation in dependence of the probing depth is shown.

Parts of this research were carried out at PETRA III beamline P09 at DESY, a member of the Helmholtz Association (HGF). We would like to thank A. Gloskovskii for assistance in using the HAXPEEM instrument. The authors thank C. Bäumer for fruitful discussions. This work was in part funded by the German Research Foundation (DFG) under Grant No. SFB 917. R.D. also acknowledges funding from the W2/W3 program of the Helmholtz association.

[1] R. Waser and M. Aono, Nat. Mater. **6**, 833 (2007).
[2] R. Waser, R. Dittmann, G. Staikov, and K. Szot, Adv. Mater. **21**, 2632 (2009).
[3] H. S. P. Wong, L. Heng-Yuan, Y. Shimeng, C. Yu-Sheng, W. Yi, C. Pang-Shiu, L. Byoungil, F. T. Chen, and T. Ming-Jinn, Proc. IEEE **100**, 1951 (2012).
[4] C. Baeumer, R. Valenta, C. Schmitz, A. Locatelli, T. O. Mentes, S. P. Rogers, A. Sala, N. Raab, S. Nemsak, M. Shim, C. M. Schneider, S. Menzel, R. Waser, and R. Dittmann, ACS Nano **11**, 6921 (2017).
[5] C. Baeumer, C. Schmitz, A. Marchewka, D. N. Mueller, R. Valenta, J. Hackl, N. Raab, S. P. Rogers, M. I. Khan, S. Nemsak, M. Shim, S. Menzel, C. M. Schneider, R. Waser, and R. Dittmann, Nat. Commun. **7**, 12398 (2016).
[6] C. Baeumer, C. Schmitz, A. H. H. Ramadan, H. Du, K. Skaja, V. Feyer, P. Muller, B. Arndt, C. Jia, J. Mayer, R. A. De Souza, C. M. Schneider, R. Waser, and R. Dittmann, Nat. Commun. **6**, 9610 (2015).
[7] D. Carta, A. P. Hitchcock, P. Guttmann, A. Regoutz, A. Khiat, A. Serb, I. Gupta, and T. Prodromakis, Sci. Rep. **6**, 21525-1 (2016).
[8] S. Kumar, C. E. Graves, J. P. Strachan, E. M. Grafals, A. L. D. Kilcoyne, T. Tyliszczak, J. N. Weker, Y. Nishi, and R. S. Williams, Adv. Mater. **28**, 2772 (2016).
[9] F. Miao, J. P. Strachan, J. J. Yang, M.-X. Zhang, I. Goldfarb, A. C. Torrezan, P. Eschbach, R. D. Kelly, G. Medeiros-Ribeiro, and R. S. Williams, Adv. Mater. **23**, 5633 (2011).
[10] D. Cooper, C. Baeumer, N. Bernier, A. Marchewka, C. La Torre, R. E. Dunin-Borkowski, S. Menzel, R. Waser, and R. Dittmann, Adv. Mater. **29**, 1700212 (2017).
[11] P. Calka, E. Martinez, V. Delaye, D. Lafond, G. Audoit, D. Mariolle, N. Chevalier, H. Grampeix, C. Cagli, V. Jousseaume, and C. Guedj, Nanotechnology **24**, 85706-1 (2013).
[12] C. Lenser, R. Dittmann, and J.-P. Strachan, "Valence Change Observed by Nanospectroscopy and Spectromicroscopy," in *Resistive Switching: From Fundamentals of Nanoionic Redox Processes to Memristive Device Application*, edited by D. Ielmini and R. Waser (Wiley, 2016).
[13] C. Baeumer, N. Raab, T. Menke, C. Schmitz, R. Rosezin, P. M. Müller, M. Andrä, V. Feyer, R. Bruchhaus, F. Gunkel, C. M. Schneider, R. Waser, and R. Dittmann, Nanoscale **8**, 13967 (2016).
[14] K. Skaja, C. Bäumer, O. Peters, S. Menzel, M. Moors, H. Du, M. Bornhöfft, C. Schmitz, C.-L. Jia, C. M. Schneider, J. Mayer, R. Waser, and R. Dittmann, Adv. Funct. Mater. **25**, 7154 (2015).
[15] R. Dittmann, R. Muenstermann, I. Krug, D. Park, T. Menke, J. Mayer, A. Besmehn, F. Kronast, C. M. Schneider, and R. Waser, Proc. IEEE **100**, 1979 (2012).
[16] L. A. Walsh, G. Hughes, P. K. Hurley, J. Lin, and J. C. Woicik, Appl. Phys. Lett. **101**, 241602-1 (2012).
[17] M. Sacchi, F. Offi, P. Torelli, A. Fondacaro, C. Spezzani, M. Cautero, G. Cautero, S. Huotari, M. Grioni, R. Delaunay, M. Fabrizioli, G. Vanko, G. Monaco, G. Paolicelli, G. Stefani, and G. Panaccione, Phys. Rev. B **71**, 155117-1 (2005).
[18] E. Slooten, Z. Zhong, H. J. A. Molegraaf, P. D. Eerkes, S. de Jong, F. Massee, E. van Heumen, M. K. Kruize, S. Wenderich, J. E. Kleibeuker, M. Gorgoi, H. Hilgenkamp, A. Brinkman, M. Huijben, G. Rijnders, D. H. A. Blank, G. Koster, P. J. Kelly, and M. S. Golden, Phys. Rev. B **87**, 85128-1 (2013).
[19] F. Borgatti, I. Bergenti, F. Bona, V. Dediu, A. Fondacaro, S. Huotari, G. Monaco, D. A. MacLaren, J. N. Chapman, and G. Panaccione, Appl. Phys. Lett. **96**, 43306-1 (2010).
[20] A. Herpers, C. Lenser, C. Park, F. Offi, F. Borgatti, G. Panaccione, S. Menzel, R. Waser, and R. Dittmann, Adv. Mater. **26**, 2730 (2014).
[21] M. Sowinska, T. Bertaud, D. Walczyk, S. Thiess, M. A. Schubert, M. Lukosius, W. Drube, C. Walczyk, and T. Schroeder, Appl. Phys. Lett. **100**, 233509 (2012).
[22] D. Carta, G. Mountjoy, A. Regoutz, A. Khiat, A. Serb, and T. Prodromakis, J. Phys. Chem. C **119**, 4362 (2015).
[23] R. Waser, R. Bruchhaus, and S. Menzel, "Redox-based resistive switching memories," in *Nanoelectronics and Information Technology*, 3rd ed. (Wiley-VCH, 2012), pp. 683–710.
[24] P. Parreira, G. W. Paterson, S. McVitie, and D. A. MacLaren, J. Phys. D: Appl. Phys. **49**, 95111-1 (2016).
[25] A. Wedig, M. Luebben, D.-Y. Cho, M. Moors, K. Skaja, V. Rana, T. Hasegawa, K. Adepalli, B. Yildiz, R. Waser, and I. Valov, Nat. Nanotechnol. **11**, 67 (2016).
[26] T. Bertaud, M. Sowinska, D. Walczyk, S. Thiess, A. Gloskovskii, C. Walczyk, and T. Schroeder, Appl. Phys. Lett. **101**, 143501-1 (2012).
[27] W. Kim, S. Menzel, D. J. Wouters, Y. Guo, J. Robertson, B. Rösgen, R. Waser, and V. Rana, Nanoscale **8**, 17774 (2016).
[28] U. Celano, J. Op de Beeck, S. Clima, M. Luebben, P. M. Koenraad, L. Goux, I. Valov, and W. Vandervorst, ACS Appl. Mater. Interfaces **9**, 10820–10824 (2017).
[29] U. Celano, L. Goux, R. Degraeve, A. Fantini, O. Richard, H. Bender, M. Jurczak, and W. Vandervorst, Nano Lett. **15**, 7970 (2015).
[30] M. Escher, N. Weber, M. Merkel, B. Kromker, D. Funnemann, S. Schmidt, F. Reinert, F. Forster, S. Hufner, P. Bernhard, D. Ziethen, H. Elmers, and G. Schonhense, J. Electron Spectrosc. Relat. Phenom. **144**, 1179 (2005).
[31] C. Wiemann, M. Patt, S. Cramm, M. Escher, M. Merkel, A. Gloskovskii, S. Thiess, W. Drube, and C. M. Schneider, Appl. Phys. Lett. **100**, 223106-1 (2012).
[32] M. Patt, C. Wiemann, N. Weber, M. Escher, A. Gloskovskii, W. Drube, M. Merkel, and C. M. Schneider, Rev. Sci. Instrum. **85**, 113704 (2014).
[33] J. Strempfer, S. Francoual, D. Reuther, D. K. Shukla, A. Skaugen, H. Schulte-Schrepping, T. Kracht, and H. Franz, J. Synchrotron Radiat. **20**, 541 (2013).
[34] J. Walton and N. Fairley, J. Electron Spectrosc. Relat. Phenom. **148**, 29 (2005).
[35] C. Morant, J. Sanz, L. Galan, L. Soriano, and F. Rueda, Surf. Sci. **218**, 331 (1989).
[36] J. H. Scofield, "Theoretical Photoionization Cross Sections From 1 to 1500 keV," Report No. UCRL–51326, Lawrence Livermore Laboratory, University of California, Livermore, California, 2013.
[37] B. Diaz, J. Swiatowska, V. Maurice, A. Seyeux, E. Härkönen, M. Ritala, S. Tervakangas, J. Kolehmainen, and P. Marcus, Electrochim. Acta **90**, 232 (2013).

[38] O. Kerrec, D. Devilliers, H. Groult, and P. Marcus, Mater. Sci. Eng.: B **55**, 134 (1998).
[39] Y. Y. Chen, G. Pourtois, S. Clima, L. Goux, B. Govoreanu, A. Fantini, R. Degraeve, G. S. Kar, G. Groeseneken, D. J. Wouters, and M. Jurczak, ECS Trans. **50**, 3 (2013).
[40] R. Yang, K. Terabe, T. Tsuruoka, T. Hasegawa, and M. Aono, Appl. Phys. Lett. **100**, 231603-1 (2012).
[41] D. S. Jeong, H. Schroeder, and R. Waser, Phys. Rev. B **79**, 195317-1 (2009).
[42] Y. Wang, X. Qian, K. Chen, Z. Fang, W. Li, and J. Xu, Appl. Phys. Lett. **102**, 042103 (2013).
[43] A. Mehonic, M. Buckwell, L. Montesi, M. S. Munde, D. Gao, S. Hudziak, R. J. Chater, S. Fearn, D. McPhail, M. Bosman, A. L. Shluger, and A. J. Kenyon, Adv. Mater. **28**, 7549 (2016).
[44] P. Gao, Z. Wang, W. Fu, Z. Liao, K. Liu, W. Wang, X. Bai, and E. Wang, Micron **41**, 301 (2010).
[45] M. Moors, K. K. Adepalli, Q. Lu, A. Wedig, C. Bäumer, K. Skaja, B. Arndt, H. L. Tuller, R. Dittmann, R. Waser, B. Yildiz, and I. Valov, ACS Nano **10**, 1481 (2016).
[46] R. Ortega-Hernandez, M. Coll, J. Gonzalez-Rosillo, A. Palau, X. Obradors, E. Miranda, T. Puig, and J. Sune, Microelectron. Eng. **147**, 37 (2015).
[47] M. Scherff, B. Meyer, J. Hoffmann, C. Jooss, M. Feuchter, and M. Kamlah, New J. Phys. **17**, 033011 (2015).
[48] L. Goux, P. Czarnecki, Y. Y. Chen, L. Pantisano, X. P. Wang, R. Degraeve, B. Govoreanu, M. Jurczak, D. J. Wouters, and L. Altimime, Appl. Phys. Lett. **97**, 243509 (2010).
[49] H. Tian, H.-Y. Chen, G. Gao, S. Yu, J. Liang, Y. Yang, D. Xie, J. F. Kang, T.-L. Ren, Y. Zhang, and H.-S. P. Wong, Nano Lett. **13**, 651 (2013).